frontiers in Marine Science

ORIGINAL RESEARCH
published: 04 February 2021
doi: 10.3389/fmars.2021.607083

Molecular Traits of Dissolved Organic Matter in the Subterranean Estuary of a High-Energy Beach: Indications of Sources and Sinks

Hannelore Waska[1], Heike Simon[1], Soeren Ahmerkamp[2], Janek Greskowiak[3], Janis Ahrens[4], Stephan L. Seibert[3], Kai Schwalfenberg[5], Oliver Zielinski[5,6] and Thorsten Dittmar[1,7]*

[1] Research Group for Marine Geochemistry (ICBM-MPI Bridging Group), Institute for Chemistry and Biology of the Marine Environment, University of Oldenburg, Oldenburg, Germany, [2] Max Planck Institute for Marine Microbiology, Bremen, Germany, [3] Hydrogeology and Landscape Hydrology Group, Institute for Biology and Environmental Sciences, University of Oldenburg, Oldenburg, Germany, [4] Microbiogeochemistry Group, Institute for Chemistry and Biology of the Marine Environment, University of Oldenburg, Oldenburg, Germany, [5] Marine Sensor Systems Group, Institute for Chemistry and Biology of the Marine Environment, University of Oldenburg, Oldenburg, Germany, [6] Marine Perception Research Group, German Research Center for Artificial Intelligence, Oldenburg, Germany, [7] Helmholtz Institute for Functional Marine Biodiversity at the University of Oldenburg, Oldenburg, Germany

OPEN ACCESS

Edited by:
Clare Robinson, University of Western Ontario, Canada

Reviewed by:
Martin Andersen, University of New South Wales, Australia
Gwénaëlle Chaillou, Université du Québec à Rimouski, Canada

***Correspondence:**
Hannelore Waska
hannelore.waska@uni-oldenburg.de

Specialty section:
This article was submitted to Marine Biogeochemistry, a section of the journal Frontiers in Marine Science

Received: *16 September 2020*
Accepted: *13 January 2021*
Published: *04 February 2021*

Citation:
Waska H, Simon H, Ahmerkamp S, Greskowiak J, Ahrens J, Seibert SL, Schwalfenberg K, Zielinski O and Dittmar T (2021) Molecular Traits of Dissolved Organic Matter in the Subterranean Estuary of a High-Energy Beach: Indications of Sources and Sinks. Front. Mar. Sci. 8:607083. doi: 10.3389/fmars.2021.607083

Advective flows of seawater and fresh groundwater through coastal aquifers form a unique ecohydrological interface, the subterranean estuary (STE). Here, freshly produced marine organic matter and oxygen mix with groundwater, which is low in oxygen and contains aged organic carbon (OC) from terrestrial sources. Along the groundwater flow paths, dissolved organic matter (DOM) is degraded and inorganic electron acceptors are successively used up. Because of the different DOM sources and ages, exact degradation pathways are often difficult to disentangle, especially in high-energy environments with dynamic changes in beach morphology, source composition, and hydraulic gradients. From a case study site on a barrier island in the German North Sea, we present detailed biogeochemical data from freshwater lens groundwater, seawater, and beach porewater samples collected over different seasons. The samples were analyzed for physico-chemistry (e.g., salinity, temperature, dissolved silicate), (reduced) electron acceptors (e.g., oxygen, nitrate, and iron), and dissolved organic carbon (DOC). DOM was isolated and molecularly characterized via soft-ionization ultra-high-resolution mass spectrometry, and molecular formulae were identified in each sample. We found that the islands' freshwater lens harbors a surprisingly high DOM molecular diversity and heterogeneity, possibly due to patchy distributions of buried peat lenses. Furthermore, a comparison of DOM composition of the endmembers indicated that the Spiekeroog high-energy beach STE conveys chemically modified, terrestrial DOM from the inland freshwater lens to the coastal ocean. In the beach intertidal zone, porewater DOC concentrations, lability of DOM and oxygen concentrations, decreased

while dissolved (reduced) iron and dissolved silicate concentrations increased. This observation is consistent with the assumption of a continuous degradation of labile DOM along a cross-shore gradient, even in this dynamic environment. Accordingly, molecular properties of DOM indicated enhanced degradation, and "humic-like" fluorescent DOM fraction increased along the flow paths, likely through accumulation of compounds less susceptible to microbial consumption. Our data indicate that the high-energy beach STE is likely a net sink of OC from the terrestrial and marine realm, and that barrier islands such as Spiekeroog may act as efficient "digestors" of organic matter.

Keywords: high-energy beach, dissolved organic matter, subterranean estuary, porewater, barrier island, North Sea, coastal aquifer

INTRODUCTION

Subterranean estuaries (STEs) underlying beaches are underground mixing zones of fresh, meteoric groundwater with seawater, which is pumped through the beach aquifer by waves and tides (Moore, 1999). Porewater flow constantly supplies the beach aquifer with organic matter and electron acceptors, making STEs highly active biogeochemical reactors (Anschutz et al., 2009). Along these advective flowpaths, organic matter is degraded and remineralization products accumulate, before they enter the coastal ocean as submarine groundwater discharge (SGD). Therefore, STEs are characterized by both strong salinity and redox gradients (Rocha, 2008; Reckhardt et al., 2015).

Since the turn of the millennium, the steadily growing recognition of STEs as global, ubiquitous land-ocean interfaces (Ma and Zhang, 2020) has led to a wealth of investigations (e.g., Charette and Sholkovitz, 2006; Robinson et al., 2006; Santos et al., 2009; Roy et al., 2010; Kim et al., 2012; Beck et al., 2017). In particular, the topic of sources and fate of organic matter in STEs has received increasing attention in the past decade, as organic matter is the fuel that drives the STE microbial biogeochemical reactor. Especially, novel spectrophotometric and mass spectrometric techniques have elucidated organic matter inputs and processing in subterranean estuaries (e.g., Kim et al., 2012; Seidel et al., 2015; Suryaputra et al., 2015; Jiang et al., 2020; McDonough et al., 2020a).

Most STEs receive aged dissolved organic matter (DOM) of low bioavailability from soils via the fresh groundwater endmember. However, fresh groundwater in a beach STE can also be a carrier of marine DOM from beach wrack and other particulate organic matter (POM; Santos et al., 2009; Suryaputra et al., 2015; Kim et al., 2019). The seawater endmember provides newly produced DOM from phytoplankton, which is considered more bioavailable compared to aged, groundwater-derived DOM (Seidel et al., 2015). In addition, recirculating seawater was found to leach and transport DOM from particulate marine organic matter buried in the sediment (Kim et al., 2019), as well as from terrestrial paleosols (Seidel et al., 2014; Couturier et al., 2016).

In microtidal, sheltered beaches with a high hydraulic gradient from inland groundwater, terrestrial DOM can be supplied to the STE in large proportions (McAllister et al., 2015; Couturier et al., 2016; Meredith et al., 2020). Contrastingly, in meso-to macrotidal regions, large volumes of marine, labile DOM are pumped through the STE, with models predicting seawater infiltrations up to several tens of meters depth into the beach aquifer (Robinson et al., 2006; Grünenbaum et al., 2020). On the global scale, the volumes of seawater-SGD are several fold higher than those of the fresh groundwater flux (Santos et al., 2012; Kwon et al., 2014; Luijendijk et al., 2020; note that the latter authors did not take into account tidally recirculated fluxes). Taking marine DOM and POM, coastal paleosols, and coastal beach wrack into account, a high-volume throughput of the marine endmember will therefore largely define the source functions and processing of both, terrestrial and marine DOM, in STEs worldwide. Yet, only a few studies of organic matter inputs into meso-to macrotidal STEs are available to date (e.g., Goñi and Gardner, 2003; Kim et al., 2012; Seidel et al., 2015), and only two of those have investigated a site additionally exposed to high-energy waves (Reckhardt et al., 2015; Beck et al., 2017).

Once DOM has entered the STE from different sources, it is abiotically or biologically processed, for example by adsorption/desorption to/from mineral phases, and microbial respiration, respectively. Adsorption of DOM on iron minerals occurs when source water flows through sediments which are rich in iron oxides, and DOM compounds are filtered out (Kaiser and Guggenberger, 2000). DOM may also co-precipitate with iron at oxic-anoxic interfaces commonly found in STEs (Linkhorst et al., 2017; Sirois et al., 2018). Both processes are compound-selective, targeting comparatively less saturated, more aromatic compounds with high oxygen content (Riedel et al., 2012). In addition, they are reversible and may release DOM once reduced conditions are restored (Lalonde et al., 2012; Linkhorst et al., 2017), therefore posing a transient storage pool of organic matter. So far, data on DOM-iron mineral interactions in STEs are scarce (Linkhorst et al., 2017; Sirois et al., 2018). Hence, the magnitudes, and temporal and spatial dynamics of these processes are not well known.

On the biological side, microbes feed on DOM and sequentially consume electron acceptors based on energy yield from oxygen to nitrate, manganese and iron oxides, sulfate, and finally inorganic carbon (Froelich et al., 1979). In parallel to the sequential exhaustion of the electron acceptors, organic matter too is assumed to be degraded along an intrinsic reactivity continuum (Benner and Amon, 2015). As a result,

along the advective flowpath in the STE, accumulation of reduced electron acceptors is accompanied by a decrease in the (relative) abundance of more bioavailable, saturated compounds and carbohydrates, and an increase of abundances of less bioavailable, less saturated, more aromatic compounds (Seidel et al., 2015; Beck et al., 2017). In reactive transport models, this degradation is acknowledged in a simplified manner, attributing decreasing reactivity to increasing age of organic matter (Van Cappellen and Wang, 1996; Spiteri et al., 2008; Anderson et al., 2019). However, heterogeneous flow patterns and additions of DOM from buried patches of POM can disrupt continuous degradation pathways and produce a non-steady state DOM distribution (Rocha, 2008; Santos et al., 2009; Kim et al., 2019). Therefore, more qualitative and quantitative data on DOM sources and sinks are needed to assess and predict organic matter turnover in the STE and calibrate site-specific reactive transport models. Another uncertainty is associated with temporal and spatial dynamics of physical disturbances, and how they might impact the efficiency of the STE microbial community to degrade DOM. In sheltered environments, DOM appears to accumulate along advective water flowpaths due to increasing degradation of POM while at the same time energy-rich electron acceptors are consumed and not replenished fast enough (Roy et al., 2011; Seidel et al., 2014). On the other hand, wave action and large tidal amplitudes may speed up organic matter respiration due to high oxygen supply via sediment re-distribution and fast water circulation. The question is then, whether too high disturbance amplitudes or frequencies, for example by storm events or high-energy waves, have a negative influence on the adaptation capacities of the microbial community. So far, a comparison of research literature from different types of environments indicates that frequent disturbances of flow paths and sediment structures enhance, rather than restrict, microbial remineralization processes in high-energy STEs (McLachlan, 1982; Charbonnier et al., 2013; Reckhardt et al., 2015; Ibánhez and Rocha, 2016; Waska et al., 2019b). If there is no upper limit to microbial resilience against physical disturbances (Novitsky and MacSween, 1989; Degenhardt et al., 2020), then meso- to macrotidal STEs with strong wave action should be particularly active sites of organic matter turnover along the world's coastlines.

In this study, we set out to investigate DOM sources and sinks in a mesotidal, high-energy beach STE on Spiekeroog Island. This STE is characterized by a rather uniform geology and (terrestrial) hydrology (Röper et al., 2012), but complex tidal, wave, and storm flood patterns on the marine side (Beck et al., 2017). Previous research at the study site hinted at a surprisingly high DOM heterogeneity in groundwater, probably stemming from ancient peat layers and surficial influences of dune vegetation (Beck et al., 2017). In 2019, we reported so far unknown brackish porewater patches at the low water line, and suggested that they stem from inland groundwater (Waska et al., 2019b). Furthermore, a decrease of DOC concentrations along the underground flowpaths was attributed to rapid remineralization, indicating that this site may be a net sink for organic carbon (OC; Reckhardt et al., 2015). Therefore, we set out to answer the following questions: (1) What are the molecular signatures of the various types of terrigenous DOM on the island, and are they comparable to those found in brackish porewaters at the low water line? (2) What are the likely abiotic and biotic sinks of DOM, and can they be disentangled by characteristic molecular traits? (3) Is this high-energy, mesotidal system a net source or net sink of organic matter to the coastal North Sea?

To answer these questions, we conducted endmember sampling of seawater, groundwater, and porewater over four sampling campaigns across different seasons and tied their molecular DOM characteristics to electron acceptor distributions and dynamics (Ahrens et al., 2020). In addition, we investigated the co-evolution of DOC and DOM with the accumulation of the groundwater-tracer dissolved silicate (DSi; Oehler et al., 2019) and a DOM fluorescence marker which is known to accumulate in aged groundwater (Nelson et al., 2015; Kim and Kim, 2017). Finally, we investigated DOC and DOM release from the shallow STE over a tidal cycle in two different seasons. The assembly of these large and diverse datasets has enabled us to provide a comprehensive picture of DOM sources and sinks in the shallow STE.

MATERIALS AND METHODS

Study Site

Our study site is located on the northern coast of Spiekeroog Island, which is part of a barrier island chain in the southern North Sea at the German coast of Lower Saxony (**Figure 1A**). The islands' freshwater lens (**Figure 1B**), as well as the beach site itself, have been subject to numerous investigations (for example Röper et al., 2012; Reckhardt et al., 2015; Beck et al., 2017; Reckhardt et al., 2017; Seibert et al., 2018, 2019a; Waska et al., 2019a,b; Ahrens et al., 2020). Briefly, the beach aquifer consists of medium- to fine-grained sands. A clay layer borders the freshwater lens at ∼40–50 meter below sea level (mbsl), but it is not known whether it extends underneath the whole beach aquifer as well (cf., Röper et al., 2012, and references cited therein). The beach length from dune base to low water line is approximately 200–300 m. In the intertidal zone, a shore-parallel runnel can be found downslope of the high water line, then the beach ascends to a ridge before descending toward the low water line (**Figures 1C**, **2**). Both, ridge and runnel undergo strong topographic changes due to wave impact and winter storm floods (Waska et al., 2019b). Numeric models, as well as *in situ* porewater sampling campaigns, indicated that groundwater from the inland fresh water lens exfiltrates into the runnel as well as into the surf zone at the low water line (Beck et al., 2017; Grünenbaum et al., 2020). The high water line and ridge serve as main seawater infiltration zones, which drain into runnel and low water line during receding tide (**Figure 2**). Several studies have characterized the inorganic and organic geochemistry of the study site (e.g., Reckhardt et al., 2015; Beck et al., 2017; Waska et al., 2019b; Ahrens et al., 2020; Paffrath et al., 2020). Overall, the upper intertidal zone between high water line and runnel is dominated by a

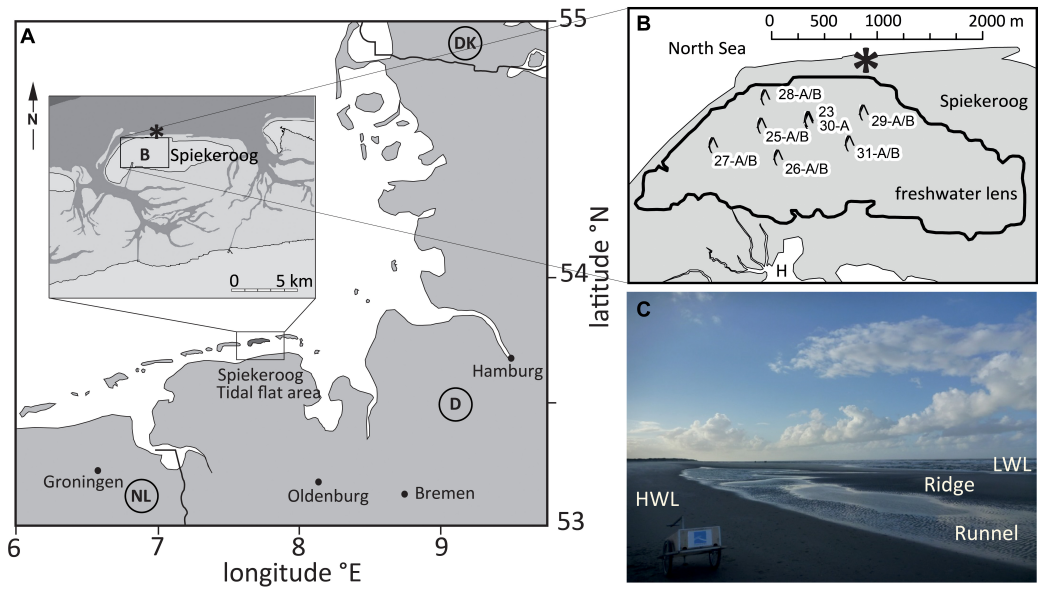

FIGURE 1 | (A) Location of Spiekeroog Island in the German North Sea. **(B)** Enlarged map of box B, with central Spiekeroog in gray and the surrounding sea in white (H = Harbour of Spiekeroog, which faces the Wadden Sea to the South). The black line indicates the borders of the freshwater lens. The well sites sampled for this study are marked with a symbol and with numbers (modified from Seibert et al., 2018). The asterisk denotes the beach sampling site. **(C)** Typical beach morphology. HWL, high water line; LWL, low water line.

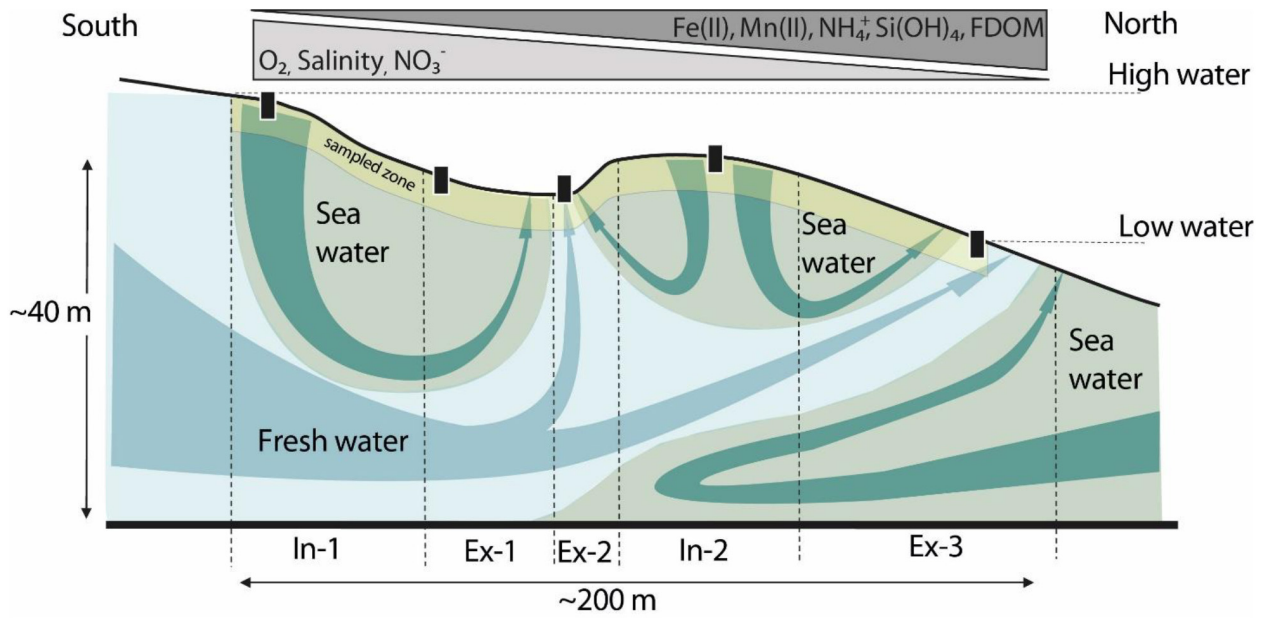

FIGURE 2 | Schematic diagram of a beach cross-section at the study site, modified from Waska et al. (2019b) and Ahrens et al. (2020). The landward side is South, the North faces the open North Sea. The gray–blue arrows depict flow from the islands fresh water lens, the green arrows show seawater circulation through the beach aquifer. In-1 and Ex-3 bracket the intertidal zone of the beach. The triangles on top indicate the direction in which the respective constituent concentrations increase, i.e., concentrations of reduced compounds increase toward the low water line. The yellow section is an approximation of the sampling depths covered in this study compared to the overall extent of the beach aquifer. Black boxes indicate the location of the transect stations. A detailed map of the transect points can be found in Ahrens et al. (2020), **Figure 1C** and Degenhardt et al. (2020), **Figure 1**.

sharp oxic gradient. Between runnel and ridge, active nitrogen cycling (denitrification–nitrification) takes place, while Mn and Fe reduction prevail from the ridge toward the low water line. The horizontal succession of electron acceptors expands across the beachface width during winter and contracts during summer, thus shifting the borders of redox zones in

the cross-shore direction between high and low water line (Ahrens et al., 2020).

Sampling

Intertidal Transects

Samples were collected in four campaigns: October 2016, March 2017, August 2017, and February 2018. With the exception of the March 2017 campaign, all campaigns took place during spring tide. In October 2016, porewaters from two cross-shore transects, approximately 60 m apart, with five stations and four depths (10, 30, 50, and 100 cm below surface) each were sampled. These stations spanned across the whole intertidal zone and covered the main morphological features (e.g., high water line, runnel, ridge, and low water line) and associated in-and exfiltration zones (Waska et al., 2019b). Further details on transect locations and sampling point distributions can be found in Ahrens et al. (2020), **Figure 1C**, and Degenhardt et al. (2020), **Figure 1**. Several stations from the October campaign were re-visited in March and August. Additionally, a third transect, parallel to the other two, was sampled ∼200 m further eastward in March 2017. In February 2018, transect sampling occurred in the vicinity of the most westward transect from October, but not at the exact same stations.

At the sampling stations, porewater was drawn using polyethylene (PE) syringes and stainless steel push-point samplers. Temperature, conductivity, oxygen, and fluorescent DOM (FDOM, excitation center-wavelength 375 nm, emission wavelength range >420 nm) were measured on site using hand-held multimeters (WTW Multi 3430/WTW pH/Cond 340i with TetraCon 925 Conductivity Sensor; FireStingGO2, Pyro-Science; Aquafluor, Turner Instruments). Details on instrument calibration can be found in Waska et al. (2019b) and Ahrens et al. (2020). FDOM measurements were conducted with filtered samples using Whatman Acrodisc GHP 0.2 μm syringe filters. Porewater samples for nutrients and trace metal analyses were collected with the syringes, filtered directly into low-density polyethylene (LDPE) bottles with 0.45 μm cellulose acetate syringe filters, and poisoned with mercury chloride (nutrients) or acidified with ultra-clean HNO_3 to 1% (v/v) (trace metals, Ahrens et al., 2020). For DOC and DOM, porewater samples were collected from the samplers with a 12V-battery driven ceramic piston pump (Fluid Metering, Inc., NY, United States) and Norprene chemical tubing, and directly filtered into acid-washed high-density polyethylene (HDPE) sample bottles. The polypropylene (PP) inline filter holders were equipped with a sandwich of 0.8/0.2 μm acid-washed SUPOR filter membranes (Pall). From each station, 200 mL sample volumes were collected. Filtered samples were acidified with suprapur HCl to pH 2 in a University-associated local laboratory on Spiekeroog (Umweltzentrum Wittbülten) after each day of sampling, and stored in the dark at 4°C. In total, we extracted a maximum of ∼400 mL from each sampling depth for line purging, *in situ* measurements, and samples for processing in the laboratory. Using a sediment porosity of 0.3 (Grünenbaum et al., 2020), this would correspond to a sampling halo with a radius of ∼7 cm. Therefore, we assume that the sample radii of the different depths did not overlap substantially.

Seawater and Groundwater Endmembers

Seawater samples were collected from the nearshore surf zone using acid-washed Nalgene 2 L polycarbonate (PC) bottles, and kept onsite in cool boxes. They were either filtered in between porewater stations during the day, or at the end of the sampling day in the laboratory, using the same pump and filter setup as the porewater samples. In September 2016, groundwater samples were extracted from eight monitoring wells located at different depths (∼6–40 m) in the unconfined aquifer of the islands' freshwater lens (**Figure 1B**; Seibert et al., 2018). The direct distance between the well locations and the beach sampling site ranged from ∼900 to 1,400 m (**Figure 1B**). Fourteen samples were collected in total, which were not filtered but directly acidified, and stored cool in the dark (4°C). Although groundwater travel times from the wells to the beach site (range of decades) are expected to largely exceed the time scale between groundwater and beach porewater sampling campaigns (1–2 years), we acknowledge that differences in sampling dates and sample treatment (filtered vs. non-filtered) may impact DOM composition, and thus the interpretation of endmember data has to be done with caution. In August 2017, porewater was sampled from ∼2 m depth at the dune base of Spiekeroog beach. Samples from this site had a salinity of <1 and represented a shallow groundwater source to the beach STE (hereafter named "dune porewater"). They were filtered, acidified, and stored together with the intertidal porewater samples.

Runnel Time Series

In March and September 2019, time series sampling was conducted to assess the geochemical impact of exfiltrating beach porewater on the nearshore water column. Both March and September sampling campaigns took place during morning low tides (9:58 and 9:43, respectively), with spring tidal ranges (2.8 and 3.5 m, respectively). Water samples were collected from the runnel which serves as a tidal channel, draining first the seawater from tidal inundation and then increasing amounts of exfiltrating porewater as the upper sediment layers are drained. For each of the two campaigns, water from the runnel was sampled approximately every hour over one tidal cycle, filtered on site, and acidified and stored at 4°C in the dark. In the March 2019 campaign, 200 mL samples were collected, in September 60 mL samples were collected, due to a change in the solid-phase extraction procedure for DOM.

Sample Processing and Analyses

Nutrients, Trace Metals, DOC, and TDN Analyses

Details on measurement of dissolved nitrogen species, as well as dissolved Fe and Mn, are published in Ahrens et al. (2020). The data are available on PANGAEA (doi.pangaea.de/10.1594/PANGAEA.905932). Phosphate was determined spectrophotometrically according to the methods of Itaya and Ui (1966) for phosphate <2.1 μM,

and Laskov et al. (2007) for phosphate >2.1 μM. Dissolved silicate ($Si(OH)_4$) in beach samples (porewater, seawater, runnel water, and dune base groundwater) was analyzed spectrophotometrically (Grasshoff et al., 1999) with a precision and trueness better than 10%. In the groundwater samples from the inland wells, $Si(OH)_4$ was measured by ICP-OES, with a precision better than 5% and trueness better than 15%. Further, total alkalinity was analyzed using spectrophotometric method according to Sarazin et al. (1999). DOC and total dissolved nitrogen (TDN) were measured with a Shimadzu TOC-VCPH against a deep sea Atlantic reference material (Hansell Lab, FL, United States), with precision and trueness better than 5%.

Molecular Characterization of DOM

For molecular analysis of DOM, 200 mL (seawater, porewater, and groundwater) acidified samples were desalted and concentrated by solid-phase extraction with help of 200 mg Agilent BOND ELUT cartridges following the protocol by Dittmar et al. (2008). For the runnel time series of March and September 2019, 40 mL samples were extracted onto 100 mg cartridges. This change in DOM isolation procedure was implemented in the late stage of the project to decrease sample collection and processing times. After repeated (3–4x of sample volume) washing with ultrapure water (UPW) acidified with HCl to pH 2, cartridges were dried with Argon gas. All samples were then eluted from the cartridges with Optima grade methanol (Fisher Scientific) into acid-washed, methanol-conditioned 4 mL HDPE bottles, and stored at −20°C in the freezer. Thereafter, samples were analyzed on a 15 Tesla Bruker solariX XR FT-ICR-MS (Fourier transform ion cyclotron resonance mass spectrometer) equipped with an electrospray ionization (ESI) source. For analysis of the beach porewater, sea water, and groundwater endmember samples, mass spectra were acquired using hand injection. The samples were adjusted to 5 ppm DOC with a 1:1 methanol–UPW mixture, filtered through 0.2 μm PTFE filters, and measured in broadband ESI negative ionization mode, with a flow rate of 20 μL min^{-1} and an ion accumulation time of 0.2 s. For each sample, 500 scans were acquired. For analysis of runnel time series, mass spectra were acquired using a HyStar Autoanalyzer, which was installed and hyphenated to the FT-ICR-MS at a later stage of the project, and which uses a higher injection flow rate. The samples were adjusted to 2.5 ppm DOC with a 1:1 methanol-UPW mixture and then measured in broadband ESI negative ionization mode, with a flow rate of 40 μL min^{-1} and an ion accumulation time of 0.2 s. For each sample, 200 scans were acquired. Together with the samples, an in-house deep-sea reference sample (North Equatorial Pacific Intermediate Water, NEqPIW) was measured daily to control instrument drift.

Acquired mass spectra were calibrated internally against a NEqPIW-based mass list of confirmed molecular formulae with an error of <0.1 ppm. Thereafter, the mass spectra were processed using the ICBM-OCEAN freeware (Merder et al., 2020) to remove noise, align samples along matching masses, and assign unique molecular formulae to each mass. Formula assignment was done with an error of <0.5 ppm, with the elemental setting $C_{1-100}H_{1-200}O_{1-70}N_{0-6}S_{0-2}P_{0-1}$. To yield unique formula assignments, the ICBM-OCEAN program applies a hierarchy of knock-out criteria as follows: isotopologue verification > homologous series length > assignment error. All assigned unique molecular formulae were classed into distinct molecular groups based on their elemental ratios (**Supplementary Figure 1**).

Data Processing

We assembled two main datasets of DOM molecular composition and environmental parameters: Dataset one contained all groundwater, dune porewater, seawater and beach porewater samples, and dataset two contained the two runnel time series. Therefore, all data processing as described below was done on each of the two sets individually. For DOM, the acquired mass cross tables were filtered to retain only the monoisotopic mass of each assigned molecular formulae. This approach increases the relative contribution of less abundant masses, as series of ^{13}C-containing masses of more abundant compounds are removed before further statistical analyses. Thereafter, samples were normalized against the sum of their intensities. The weighed sums of molecular properties (e.g., elemental composition, compound group classification) were calculated based on the distribution of relative signal intensities in the mass spectrum. In addition, we retrieved and applied four source-based and processing-based DOM molecular indices from the literature, which had been developed previously in other environmental settings (**Supplementary Figure 1**):

i A molecular degradation index ("Ideg"), which consists of ten ubiquitous molecular formulae, and which was developed in an open ocean setting and calibrated against the $\Delta^{14}C$ radiocarbon age of DOM (Flerus et al., 2012).
ii A broad DOM lability index ("MLB_l") which considers the H/C ratio of all molecular formulae in a sample, dividing them along a "molecular lability boundary" of H/C = 1.5 (D'Andrilli et al., 2015).
iii A terrestrial index ("ITerr") consisting of 80 ubiquitous molecular formulae, which were significantly correlated with the salinity gradient of the Amazon estuary (Medeiros et al., 2016).
iv A bioproduction index ("Ibioprod") of ten ubiquitous molecular formulae which were associated with fresh DOM release from aquatic primary production in a controlled marine mesocosm (Osterholz et al., 2015; Seibt, 2017).

Statistical analyses and plotting were done in R Studio (R version 3.5.3), using the packages *vegan*, *ggplot2*, *plyr*, and *corrplot*. Multivariate statistics primarily consisted of principal coordinate (PCoA) analyses of normalized DOM mass spectra using Bray-Curtis dissimilarities. The DOM-based distributions were correlated with environmental data (e.g., geographical location, physical properties, inorganic parameters) and weighed sums of molecular properties (e.g., elemental composition, compound group classification) using *vegan*s envfit function (Oksanen et al., 2013). Co-variations between relative intensities of molecular formulae and environmental parameters [e.g., salinity, $Si(OH)_4$] were done with Spearman's rank

correlation. Group comparisons were conducted with pairwise Wilcoxon rank-sum tests.

RESULTS

Endmember Geochemistry and DOM Characteristics

Salinities increased in the order groundwater < dune porewater < beach porewater < seawater, whereas concentrations of dissolved oxygen increased in the order groundwater < beach porewater < dune porewater < seawater (**Supplementary Table 1**). Furthermore, nitrate concentrations in dune porewater were 10- to 100-fold higher, and phosphate concentrations up to 10-fold higher, compared to the other endmembers. Beach porewater displayed the highest levels of dissolved Fe and Mn concentrations compared to groundwater, dune porewater, and seawater. On the other hand, freshwater lens groundwater had the highest ranges for DOC, $Si(OH)_4$, and FDOM concentrations (**Supplementary Table 1**).

A large DOM molecular dataset (>50,000 assigned unique molecular formulae) was produced from a total of 211 samples (groundwater, dune porewater, seawater, and beach porewater). Overall, groundwater samples yielded on average the highest number of assigned molecular formulae, and seawater samples the lowest (**Supplementary Table 2**). Similarly, DOM from groundwater samples had the highest average mass, and DOM from seawater the lowest. While no distinct trend in elemental O/C ratios could be found, average H/C ratios were overall highest in seawater and lowest in dune porewater. In line with the H/C ratios, unsaturated, aliphatic compounds, as well as the indicator for molecular lability (MLB_l; D'Andrilli et al., 2015), displayed the highest values in seawater ($p < 0.001$, Wilcoxon rank-sum test between seawater and groundwater). On the other hand, indicators of less saturated compounds, for example the aromaticity index (AI.mod) and the calculated double bond equivalents (DBE) were generally lower in seawater compared to groundwater and beach porewater ($p < 0.05$, Wilcoxon rank-sum test between seawater and groundwater). The relative abundances of aromatic compound groups, and the terrestrial index (ITerr) were also lower in seawater and beach porewater compared to groundwater, and reached their maximum values in the dune porewater samples.

The freshwater lens samples displayed a large heterogeneity with regards to $Si(OH)_4$, DOC, and FDOM concentration ranges, as well as ranges of DOM molecular indices (**Figure 3**

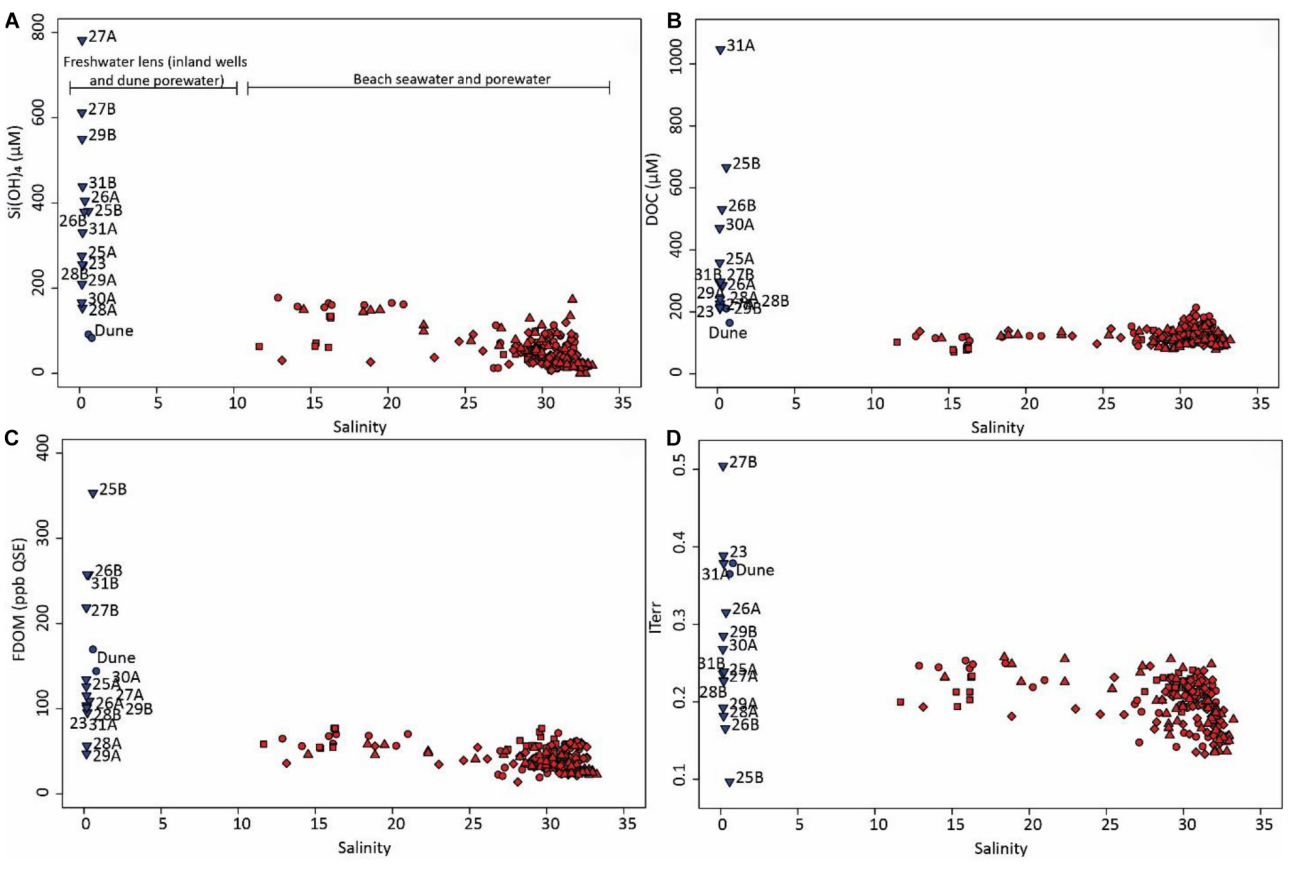

FIGURE 3 | (A) $Si(OH)_4$, **(B)** DOC, **(C)** FDOM, and **(D)** ITerr vs. salinity. The blue and red colors indicate fresh (groundwater and dune porewater) and brackish/saline (beach porewater and seawater) samples, respectively. Symbols indicate campaign season (see also **Figure 4**): Triangles = October, diamonds = March, squares = February, upside down triangles = September. Numbers indicate groundwater wells (see also **Figure 1**).

and **Supplementary Figure 2**). Spearman rank tests revealed no significant correlation of the chemical parameters with groundwater ages (Seibert et al., 2018; **Figure 4**), well locations, or well depths. In beach porewater samples, $Si(OH)_4$, and FDOM concentrations, as well as ITerr values slightly increased with decreasing salinities, while DOC concentrations were relatively low throughout (**Figure 3**). All four molecular indices were significantly correlated with DOC concentrations in beach porewaters and seawater (**Supplementary Figure 2**), most notably Ideg (**Supplementary Figure 2B**) with a $p < 0.001$ and a negative correlation coefficient of $\rho = -0.79$ (**Supplementary Figure 2B**, insert).

Via PCoA of DOM molecular composition, we condensed the extensive molecular information of all endmember water samples, i.e., relative abundances of all assigned molecular formulae, into two coordinates (PC1 and PC2). Together, the two principal coordinates explained 43.5% of DOM molecular composition. In the PCoA bivariate plot, three sample groups were distinguished along the first coordinate (PC1): A relatively compact aggregation of beach porewater samples, a widely distributed assembly of groundwater samples from the freshwater lens, and brackish beach porewater samples from the low water line plotting in between (**Figure 4**). In addition, dune porewater occupied a niche separated from the beach seawater, porewater, and groundwater samples along the second coordinate (PC2). This group was associated with high abundances of aromatic indicators (Ar, AI.mod) and ITerr. PC1 was significantly positively correlated with salinity, and significantly negatively correlated with $Si(OH)_4$ and FDOM concentrations. Seawater and beach porewater samples associated with high salinity were also linked with unsaturated compounds, particularly those containing nitrogen, and with high abundances of the lability index MLB_l. PC2 was negatively correlated with O_2 concentrations and relative abundances of highly unsaturated compounds (HU), and positively correlated with Fe and NH_4^+ concentrations, and relative abundances of aromatic compounds (Ar).

In addition to sample-specific DOM molecular fingerprints, we also found distinct molecular properties correlating (Spearman rank test) in their relative abundances to concentrations of the environmental parameters DOC, FDOM, $Si(OH)_4$, Fe, and O_2 (**Figures 5A–E**) in beach porewater and

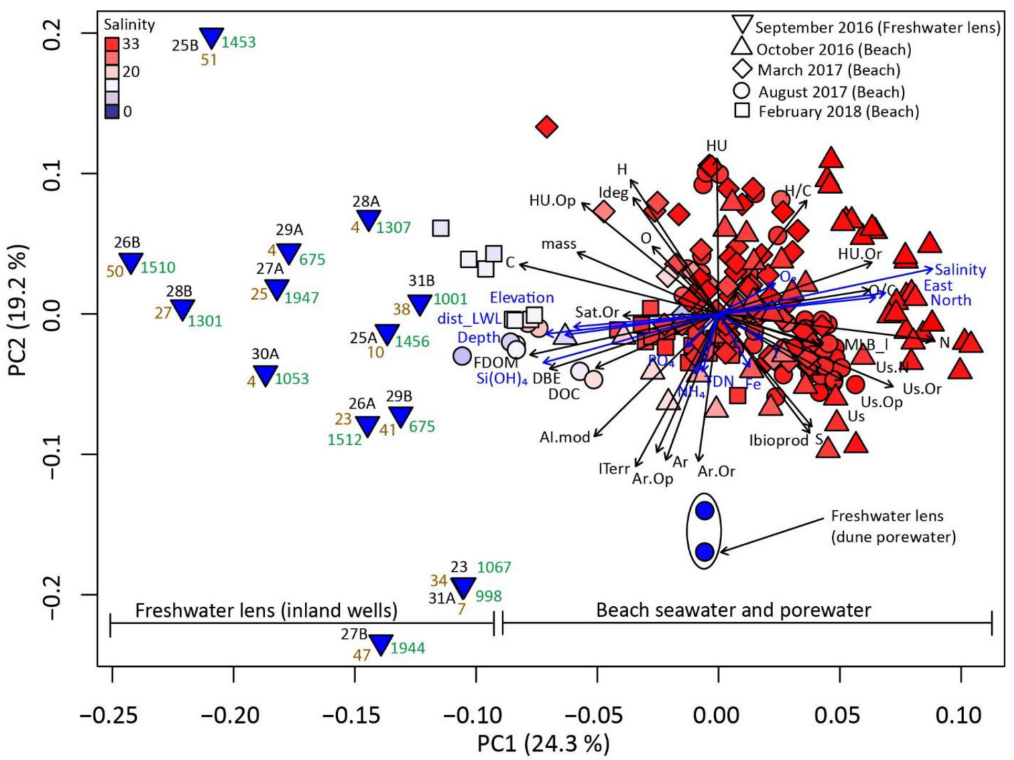

FIGURE 4 | Principal coordinate analysis (PCoA) using Bray-Curtis similarities of DOM molecular composition. Numbers next to inland well samples correspond to well locations as in **Figure 1**, with A and B indicating shallow (~6–10 mbsl) and deep (~20–40 mbsl) wells, respectively. Tan numbers denote $^3H/^3He$ dated groundwater ages (Seibert et al., 2018). Green numbers denote direct distance of well sites from the low water line. Blue arrows display significant ($p < 0.05$) correlations of environmental parameters with the principal coordinates, with the direction of the arrow indicating positive correlation, and its length indicating strength of the correlation coefficient. Environmental parameters contain geographic (Universal Transverse Mercator coordinates, elevation, sampling depth), and physico-chemical data (NH_4^+, TDN, PO_4^{3-}, $Si(OH)_4$, O_2, NO_2^-, Salinity, Mn, Temperature, Fe). Black arrows display significant ($p < 0.001$) correlations of DOC and FDOM concentrations, and chemical DOM properties (intensity-weighed) with the principal coordinates. These include (i) relative abundances of elements and elemental ratios (e.g., C, H/C, O, N) of assigned molecular formulae, (ii) relative abundances of compound classes (**Supplementary Figure 1**, e.g., Ar.Or = Aromatic oxygen-rich, HU = highly unsaturated), (iii) relative distribution of indices (e.g., AI.mod, double bond equivalents = DBE, MLB_l, ITerr).

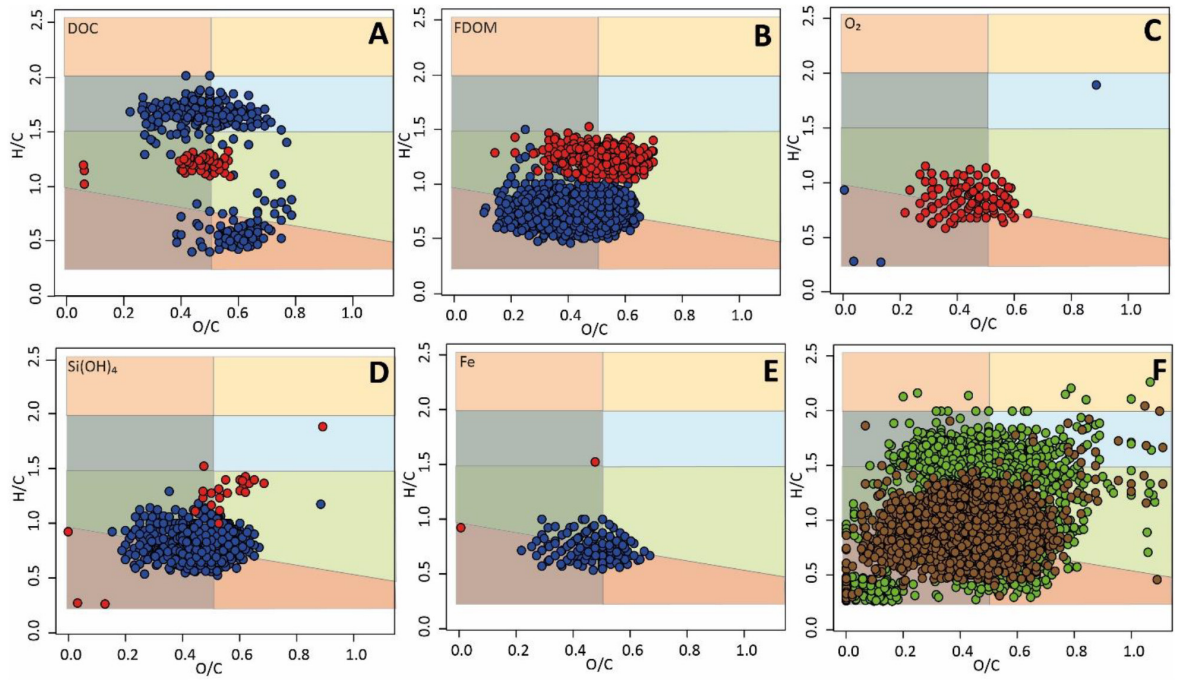

FIGURE 5 | (A–E) Van Krevelen plots of compounds significantly correlating with environmental parameters (Spearman rank test, $p < 0.05$). Blue color indicates positive correlations ($\rho > 0.5$) and red color negative correlations ($\rho < -0.5$). **(F)** van Krevelen plot of compounds associated with beach porewaters from the high water line (green color) *vs.* compounds associated with beach porewaters from the runnel (Ex-2, tan color). Only compounds are shown which are significantly higher in either compartment (Wilcoxon rank-sum test, $p < 0.05$, ratio > 1). The background colors of the plots refer to compound group classes as described in **Supplementary Figure 1A**.

seawater samples. DOC concentrations were significantly positively correlated with relative abundances of unsaturated compounds and aromatic, oxygen-rich compounds, and significantly negatively correlated with relative abundances of highly unsaturated compounds (**Figure 5A**). In contrast, FDOM, $Si(OH)_4$, and Fe concentrations were significantly positively correlated with relative abundances of aromatic compounds and highly unsaturated compounds with an H/C ratio lower than ∼1.2 (**Figures 5B,D,E**). FDOM and $Si(OH)_4$ were furthermore significantly negatively correlated with relative abundances of highly unsaturated compounds with an H/C ratio higher than ∼1.2 (**Figures 5B,D**). O_2 concentrations showed a contrasting pattern to that of FDOM, Fe, and $Si(OH)_4$ concentrations, and were significantly negatively correlated with relative abundances of aromatic compounds and highly unsaturated compounds with an H/C ratio lower than ∼1.2 (**Figure 5C**). A pairwise Wilcoxon rank-sum test comparing DOM composition in beach porewaters from the high water line (In-1) and runnel (Ex-3) revealed relative enrichment of In-1 with unsaturated and aromatic compounds, and relative enrichment of Ex-3 with highly unsaturated compounds (**Figure 5F**).

Spatial and Temporal Variations of Beach Porewater Physico-Chemistry

Seawater temperatures were 12.4°C in October, 7.5°C in March, 18.5°C in August, and 3.2°C in February. Beach porewater temperatures were 11.8 ± 1.1°C in October, 8.8 ± 1.3°C in March, 18.1 ± 0.8°C in August, and 4.5 ± 1.0°C in February. No significant differences (pairwise Wilcoxon rank-sum test, $p < 0.05$) were found between concentrations of the groundwater tracer $Si(OH)_4$ (Oehler et al., 2019) of the four sampling campaigns, although concentrations in August were slightly elevated compared to the rest (**Figure 6A**). On the other hand, $Si(OH)_4$ concentrations from all campaigns combined differed significantly between in- and exfiltration compartments in the cross-shore direction (**Figure 6B**). $Si(OH)_4$ concentrations generally increased with sampling depth (**Figure 6C**), but the differences between the depths were not statistically significant. In contrast to $Si(OH)_4$, FDOM distributions showed an overall trend of increasing concentrations from October 2016 to February 2018 (**Figure 6A**, green color code). Nevertheless, FDOM mostly co-varied with $Si(OH)_4$ on a spatial scale, and FDOM and $Si(OH)_4$ concentrations in beach porewaters were significantly positively correlated across all seasons and depths (Spearman rank test, $p < 0.001$, $\rho = 0.64$).

Dissolved organic carbon concentrations of all stations and depths were significantly different between seasons (pairwise Wilcoxon rank-sum test, $p < 0.05$), increasing in the order February < October < March < August (**Figure 7A**). In addition, DOC concentrations were significantly different amongst cross-shore compartments, with highest concentrations in seawater and lowest concentrations in Ex-2 porewater

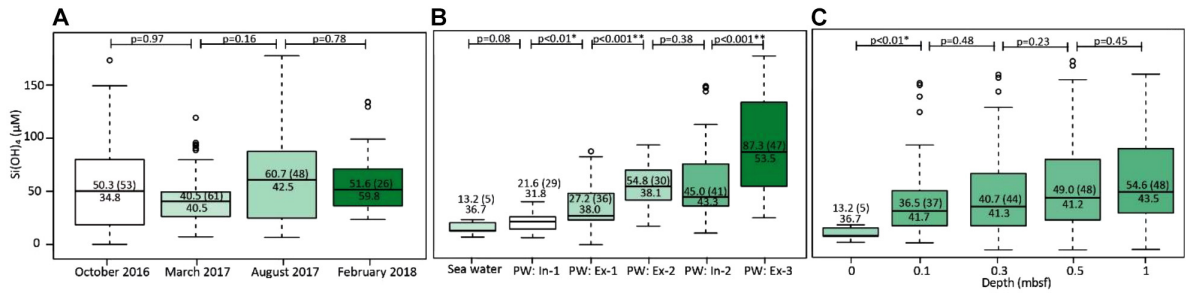

FIGURE 6 | Boxplots of $Si(OH)_4$ concentrations **(A)** for the four campaigns, **(B)** along the cross-shore transects, and **(C)** at sampled sediment depths (0 m represents seawater). Numbers next to brackets denote median $Si(OH)_4$ concentrations, numbers in brackets indicate number of samples. Numbers above display p-values for pairwise Wilcoxon rank-sum tests. The white to green color scale corresponds to increasing FDOM concentrations (also denoted by the numbers in the boxes below the median line). The captions in plot **(B)** refer to in- and exfiltration zones defined in **Figure 2**.

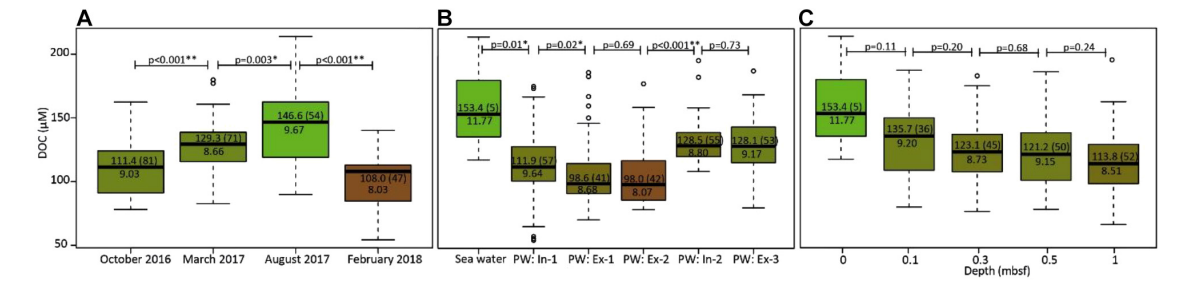

FIGURE 7 | Boxplots of DOC concentrations **(A)** for the four campaigns, **(B)** along the cross-shore transects, and **(C)** at sampled sediment depths (0 m represents seawater). Numbers next to brackets denote median DOC concentrations, numbers in brackets indicate number of samples. Numbers above display *p*-values for pairwise Wilcoxon rank-sum tests. The green to tan color scale corresponds to decreasing MLB_l values (also denoted by the numbers in the boxes below the median line). The captions in plot **(B)** refer to in- and exfiltration zones defined in **Figure 2**.

(**Figure 7B**). Overall, DOC concentrations decreased with increasing sediment depth (**Figure 7C**). Across all temporal and spatial scales, the MLB_l was significantly positively correlated with DOC concentrations (Spearman rank test, $p < 0.001$, $\rho = 0.36$).

Concentrations of total alkalinity (TA) were only determined in beach porewater, seawater, and dune porewater samples and ranged from 1.75 to 6.74 mM. They were highest in dune porewater and lowest in seawater (**Supplementary Table 1**). In beach porewater, TA was significantly negatively correlated with concentrations of dissolved O_2 (Spearman rank test, $p < 0.001$, $\rho = -0.33$), and significantly positively correlated with concentrations of dissolved Fe ($p < 0.001$, $\rho = 0.49$) and Mn $p < 0.001$, $\rho = 0.50$). Overall, highest TA concentrations were found in the August campaign (**Supplementary Figure 3A**). Analogous to $Si(OH)_4$, TA concentrations increased in beach porewaters in the cross-shore direction and with increasing sediment depth (**Supplementary Figures 3B,C**). The degradation index Ideg displayed some contrasting patterns to TA: Although it generally increased together with TA in the cross-shore direction and with increasing sediment depths, it decreased again at the infiltration zone In-2, in parallel with increasing DOC concentrations and increasing MLB_l values. Additionally, it was lowest in the August campaign when TA was highest (**Supplementary Figure 3A**).

Runnel Time Series

The runnel water temperature in March 2019 ranged between 8.3 and 8.7°C, whereas in September 2019, runnel water temperature ranged from 16.3 to 19.1°C. Overall, water levels in the runnel decreased from ∼1 m during high tide to ∼10–20 cm during low tide. During both campaigns, $Si(OH)_4$ concentrations were ∼4–6 fold higher in the runnel during low tide compared to high tide, while DOC concentrations were ∼30–40% lower (**Figures 8A,B**). Amongst DOM molecular indices, Ideg showed diverging trends, with decreasing values toward low tide in March and increasing values toward low tide in September (**Figures 8C,D**). Finally, the MLB_l decreased toward low tide in both campaigns (**Figures 8E,F**). An apparent time lag between tidal heights and temporal geochemical gradients was observed in March, but not in September (**Figures 8A–F**).

DISCUSSION

Sources of Terrestrial DOM to Spiekeroog STE

In line with a previous campaign at the same study site (Beck et al., 2017), DOM molecular composition of beach porewaters was distinctly different from that in the freshwater lens, both from inland and the dune site (**Figure 4**). Surprisingly, the DOM

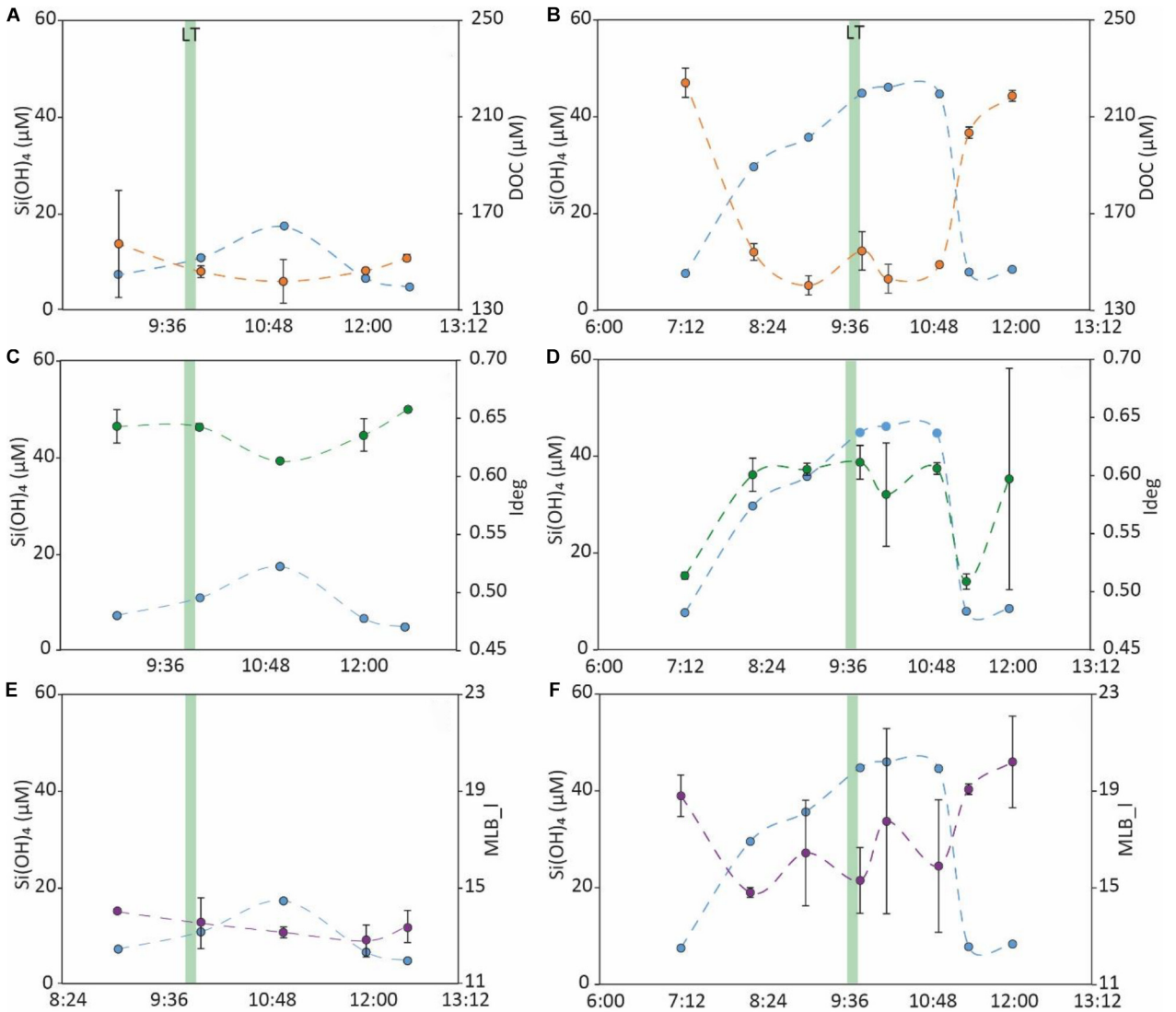

FIGURE 8 | Temporal trends in concentrations of $Si(OH)_4$, a well-known SGD tracer (Oehler et al., 2019) [light blue, **(A–F)**] and DOC [orange, **(A,B)**] and magnitudes of Ideg [green, **(C,D)**] and MLB_I [purple, **(E,F)**], in runnel water samples collected in March 2019 **(A,C,E)** and September 2019 **(B,D,F)**. The green bar indicates time of low tide.

composition in the brackish porewater sites at the low water line was more similar to that in the wells from the freshwater lens (distances of ∼600–2,000 m) compared to the samples collected from the dune base onsite (distance of ∼300 m). Therefore, at the low water line, DOM was likely a mixture of groundwater from the main lens below the island and the discharging recirculated seawater (**Figure 3**). It should be noted that amongst the groundwater well samples, there was no group or cluster formation based on e.g., location, groundwater age or sampling depth (shallow wells "A" vs. deep wells "B"). Furthermore, the wells' distances from the low water line did not appear to influence their distribution relative to the brackish low water line samples in the PCoA plot (**Figure 4**). Although the average of the terrestrial index ITerr was higher in well groundwater compared to beach porewater (**Supplementary Table 2**), it did not display a pronounced trend with salinity and differed vastly between wells (**Figure 3D**). All sampled wells are located in the same vegetation zone (Röper et al., 2012): Gray dunes, dominated by grass, for example *Corynephorus canescens,* herbaceous plants, moss, and lichens) with the exception of well 26, which is in the brown dune zone (dominance of perennial shrubs, mostly *Empetrum nigrum*). Because of the relatively homogeneous local vegetation patterns, together with the long flowpaths associated with the sampled depths (∼6-40 m) we do not assume a direct link between current plant communities and the very high DOM heterogeneity between the wells. Overall, the geology of the island consists of pre- and postglacial sand deposits, with a clay aquitard at ∼40 m depth, and peat and salt marsh deposits occurring in patches throughout the island (Streif, 2002) which likely affect groundwater well DOM composition locally. Peat porewater is

enriched in aromatic compounds compared to seawater (Riedel et al., 2012), and peat-influenced groundwater will have a higher ITerr compared to groundwater not in contact with peat, because the ITerr index is positively influenced by compounds of a higher aromaticity (Medeiros et al., 2016). Variations in the contribution of soil horizons to groundwater DOM can also influence ITerr, as topsoil DOM often has higher aromaticity compared to subsoil DOM (Shen et al., 2015; Anderson et al., 2019). On the other hand, DOM adsorption to mineral phases decreases ITerr, because it also targets more aromatic compounds of the DOM pool (Shen et al., 2015; Linkhorst et al., 2017). Originally, ITerr was developed using Amazon estuarine samples (Medeiros et al., 2016) and it may not be applicable as an unambiguous terrestrial endmember marker for subterranean estuaries. However, it could reveal mineral-water interactions along groundwater flowpaths, or be a valuable indicator of local peat or paleosol deposits in the coastal aquifer. In line with our study from the German North Sea coast, peat and/or paleosol leaching by groundwater was observed in coastal aquifers in Australia and North America (Goñi and Gardner, 2003; Couturier et al., 2016; McDonough et al., 2020b). This process can enrich coastal groundwater DOC concentrations up to tenfold compared to the global average (McDonough et al., 2020c; Meredith et al., 2020). Therefore, the transfer of ancient organic matter deposits from deep aquifers to surficial environments (with high degradation potential) could be an important process in the global coastal carbon cycle.

The similarities of DOM molecular properties between brackish beach porewater and freshwater lens groundwater were quite astonishing, and differed mainly by the much higher DOC concentrations in the latter (∼200–1,000 μM) compared to the former (∼100–150 μM). Previous research on Spiekeroog beach (and other STEs worldwide) has mainly focused on characterizing the freshwater endmember directly at the shoreline (Reckhardt et al., 2015; Seidel et al., 2015; Beck et al., 2017). In agreement with Anschutz et al. (2016), our data indicates that information about the inland watershed is necessary to constrain endmembers to the beach STE. However, a substantial unknown in our study, as well as in the current STE literature, is the fate of DOM on its transport between the inland wells and the beach STE. For example, we do not have any detailed information about the quantity and quality of the sedimentary organic matter below the dune belt. Even the particulate OC content of <0.03–0.04%% found in Spiekeroog beach sands (Beck et al., 2017; Seibert et al., 2019b) would correspond to several hundred fold higher DOC concentrations than the ones we measured in any of our samples. Therefore, it is likely that a continuous addition via the solid phase occurs along the decade-long flowpaths of the inland groundwater toward the shoreline. Based on the molecular similarities of the groundwater and brackish porewater DOM, we propose that any added DOM below the dune belt likely has comparable sedimentary sources (soils, peat, and vascular plant material) as the wells, and is processed under similar conditions. Employing a numerical density-dependent groundwater flow and transport model of the site, Grünenbaum et al. (2020) calculated a water travel time from the dune to the low water line of 16–18 years. With a mean $^{3}H/^{3}He$ age of 20–30 years of the freshwater lens (Röper et al., 2012; Seibert et al., 2018) and adding another 10–20 years to pass the STE, the mean age of the discharging fresh groundwater must be around 30–50 years. Further, numerical modeling of the reactive transport processes within the freshwater lens revealed a low sulfate reduction rate of maximum 0.015 nmol/mL/day (Seibert et al., 2019a). Therefore, it is possible, that the low availability of electron acceptors, together with the aged DOM, result in a low reactivity along the flowpath. Using this maximum sulfate reduction rate and assuming a maximum mean age of 50 years, this would yield a degradation of ∼140 μM DOC, which is less than the observed difference between the average DOC concentrations of the groundwater and beach porewater, respectively (**Supplementary Table 1**). Another DOM removal process could be adsorption onto reactive iron oxides (Linkhorst et al., 2017), which are found in small but constant amounts (∼10 mmol/kg) in surface (<2 m) sediments from our study site (Ahrens, 2016) as well as in sediment cores (up to 10 m) from a dune site in the Eastern part of the island (Seibert et al., 2019a). Considering the affinity of terrestrial, plant-derived DOM for Fe-Oxide binding, the potential of the solid phase as a (transient) storage of OC could be substantial and needs to be investigated in more detail in future studies, similar to Sirois et al. (2018). We also suspect decreases of freshwater lens-derived organic matter under the dune belt, as it mixes with dune porewater, which is in contact with the atmosphere, and which has lower DOC, higher oxygen, and higher FDOM concentrations (**Supplementary Table 1**; **Figures 3B,C**; Anschutz et al., 2016). Finally, degradation of terrestrial DOM could be accelerated once it reaches the intertidal zone, due to the deep injection of seawater rich in labile DOM ("priming"; Bianchi, 2011) and electron acceptors (e.g., oxygen, nitrate, and sulfate; Ahrens et al., 2020; Grünenbaum et al., 2020).

At the dune base, DOM was remarkably enriched with aromatic compounds compared to all other endmember samples (**Figure 4** and **Supplementary Table 2**). As we only sampled this endmember in August, it may not be representative for the remainder of the year. In the area of the dune base, so-called "Winterspülsaum" was observed, a beach wrack deposition area mainly composed of kelp (*Fucus* sp.) and dune grass (*Ammophila arenaria*) washed high up the shore during winter storms. It appears that this buried plant material, which is not reached during regular tidal inundation, influences dune porewater composition as it is leached into the aquifer by infiltrating rainwater. Unfortunately, it was not possible in the scope of this study to access deeper layers of the beach fresh groundwater endmember. Effectively, we are treating the deep beach aquifer as a "black box" of which only the infiltrating seawater, and the exfiltrating porewater (brackish and saline), are well-characterized (**Figure 2**). The relative contributions of different groundwater layers are unknown, since the brackish porewater samples contain a processed composite of groundwater from the entire freshwater lens. In a study on Spiekeroog South Beach, groundwater DOC concentrations varied between ∼100 and 400 μM over a sampling depth of only 1.5 m (Waska et al., 2019a). Little is known about vertical distributions of groundwater DOM in STEs, since spatial and temporal observations of DOC and DOM endmembers are often discussed in the context of seawater-groundwater mixing (e.g., Santos et al., 2009; Seidel et al., 2015). Most STE studies focus on the upper ∼2–3 m (e.g., Roy et al., 2010; Kim et al., 2012; Seidel et al., 2015; Yang et al., 2015;

Couturier et al., 2016) although sampling of 4 m depth or more (Charette and Sholkovitz, 2006; Beck et al., 2017; Kim et al., 2019; Meredith et al., 2020) revealed, in some cases, variations in DOC of up to 100-fold between sampling depths at the same station (Charette and Sholkovitz, 2006; Meredith et al., 2020). On Spiekeroog, the upper saline plume(s) alone reach (modeled) depths of ∼20 m (**Figure 2**; Grünenbaum et al., 2020). Therefore, probing of groundwater layers at the dune site up to 20–30 m depth may be necessary to capture all sources of terrestrial organic matter to the beach STE.

DOM Turnover in the STE

Our DOC and DOM data confirm earlier findings that seawater provides relatively fresh, labile organic matter to beach aquifers (e.g., **Figures 2**, **7** and **Supplementary Tables 1, 2**; Seidel et al., 2015). Across the beach STE, a general inverse relationship between DOC concentrations and Ideg could be found (**Supplementary Figure 2D**), whereas higher DOC concentrations were associated with higher values of molecular lability and bioproductivity indices. Environmental parameters indicative of relative water residence time in the STE in a qualitative sense, i.e., O_2, Fe, and $Si(OH)_4$ (Reckhardt et al., 2015; Oehler et al., 2019; Ahrens et al., 2020) revealed increasing relative contributions of highly unsaturated and aromatic compounds to the DOM pool with increasing porewater age. Furthermore, FDOM increased with increasing water residence times, making this fluorescence component a potential groundwater tracer as previously proposed in other coastal environments (Kim et al., 2012; Nelson et al., 2015; Kim and Kim, 2017). It should be noted that $Si(OH)_4$ and FDOM concentrations are highly influenced by the relative contributions of the fresh groundwater endmember (**Supplementary Table 1**; **Figure 6**; Ehlert et al., 2016), and that is difficult to separate patterns of accumulation along the flowpath from additions of our fresh groundwater endmember due to its large concentration ranges (**Figure 3**). On the other hand, compounds positively correlated with Fe concentrations could be not only the result of accumulation due to water age, but also from release of sedimentary OC due to reduction of reactive Fe oxides (Waska et al., 2019b).

As a general paradigm, the average H/C ratio of DOM molecular formulae is often considered an indicator of DOM lability, with compounds of H/C ratios >1.5 being degraded more rapidly than those with H/C ratios <1.5 (D'Andrilli et al., 2015), and with aromatic compounds being the most resistant to degradation due to the stability of the aromatic ring structures. However, environmental and experimental data from open ocean to freshwater environments showed that increased degradation is characterized by increased relative abundances of highly unsaturated compounds with intermediate H/C ratios of ∼1.2 and O/C ratios of ∼0.5, at the cost of both, less and more saturated compounds ("island of stability"; Lechtenfeld et al., 2014; Mostovaya et al., 2017). **Figures 5A,F** show DOM composition changes toward the "island of stability" with decreasing DOC concentrations and increasing water residence times. Therefore, degradation of both, aliphatic and aromatic compounds appears to take place in the beach STE. In addition, removal of aromatic compounds due to adsorption onto reactive iron oxides may occur along the advective porewater flowpath (Linkhorst et al., 2017; Sirois et al., 2018).

We are aware that water residence time and porewater age are inherently difficult to define in the beach STE. Based on groundwater age dating and numerical models of the local flowpaths (Röper et al., 2012; Beck et al., 2017; Grünenbaum et al., 2020), we posit that groundwater from the freshwater lens is the oldest endmember, and infiltrating seawater at the high water line the youngest, with regards to autochthonous DOM contribution. The combination of beach seawater circulation and old groundwater would then result in an overall increase of water age from high to low water line, particularly from the runnel onward, where increasing contributions of fresh groundwater are to be expected (Beck et al., 2017; Waska et al., 2019b). Tidal inundation may "reset" water age in the intertidal zone, most prominently at the ridge. Indeed, **Figures 6**, **7** show some similarities between In-1 and In-2. Nevertheless, the overall higher elevation, together with an overall higher hydraulic gradient, between high water line and runnel compared to that between ridge and low water line, seems to ensure that the largest seawater volumes are circulating through the upper intertidal zone of the beach (**Figures 2**, **5F**, **7B**). This geochemical pattern is supported by numerical models calculating fourfold higher discharge volumes in the runnel compared to the low water line (Waska et al., 2019b).

Even with fresh groundwater influence, DOC concentrations in beach porewater (across all samples and seasons) were consistently lower compared to those in both seawater (by ∼40 μM) and groundwater (by ∼160 μM when using the average of well groundwater and dune porewater, **Supplementary Table 1**). At the same time, oxygen concentrations decreased by >200 μM and nitrate concentrations by >100 μM (using average dune porewater and seawater, **Supplementary Table 1**), which would correspond to a respiration of ∼280 μM OC assuming stoichiometric reactions of only these dissolved reaction partners (Van Cappellen and Wang, 1996), and which would be more than sufficient to account for the observed loss of DOC. Of course, this very simple comparison of temporally and spatially averaged electron acceptor and electron donor budgets contains several large uncertainties: on the electron acceptor side, oxygen and nitrate participate in the chemical oxidation of reduced nitrogen, metal, and sulfur species, and could be added to shallow porewater throughout the intertidal zone via diffusion (contact with the atmosphere) as well as skin circulation during tidal inundation (Billerbeck et al., 2006; Ahmerkamp et al., 2017). Furthermore, manganese, iron, and sulfate reduction also occur on Spiekeroog beach, albeit to a lesser extent compared to oxic respiration and nitrate reduction (Ahrens et al., 2020). On the electron donor side, the concentration of the deep fresh groundwater endmember is not entirely known, and contributions of sedimentary and beach wrack OC to the porewater DOC pool could exceed DOC concentrations from sea- and groundwater by several fold in deeper (>1 m) parts of the beach STE, especially during spring and summer (Kim et al., 2019). In general, high-energy beaches are known as remineralization hot spots of marine-derived OC (McLachlan, 1982; Anschutz et al., 2009; Charbonnier et al., 2013), but the role of fresh groundwater as an additional substrate for the

beach microbial community is not well understood. In this study, our data indicate that the "aged" DOM from groundwater still undergoes degradation before it discharges into the coastal ocean. Dynamic beach hydrology could enhance microbial respiration of terrestrial DOC by supplementing the fresh groundwater endmember with oxygen, nitrate, and labile marine organic matter ("priming"; Bianchi, 2011). It is not possible to determine, based on our environmental study, which effect (supply of oxygen vs. labile OC) is more prominent on Spiekeroog beach; laboratory mesocosms are needed in future study to disentangle electron acceptor and electron donor effects on beach OC respiration.

Exfiltration of DOM and Impact on Water Column

Our runnel time series support the observations in DOC concentrations found for the different endmembers, and indicate that exfiltrating beach porewater is generally DOC-depleted compared to surface seawater (**Figure 8**). This trend occurred parallel to the reliable increase of $Si(OH)_4$, a well-known groundwater tracer (Oehler et al., 2019) during or after low tide, and was remarkably consistent in both runnel time series. Some concentration fluctuations occurred in our runnel time series data, as indicated by comparably larger standard deviations for some points in **Figure 8**. We attribute these to heterogeneities in the runnel water column, which had a dynamically changing water level and which may receive different water parcels from the draining sediments. However, such runnel time series seem to be a valuable asset to trace SGD impact in a high-energy environment where SGD-related chemical signals are diluted rather quickly by the adjacent coastal seawater. In line with our findings, a recent study on a diverse set of coastal zones, attributed dependency of STE source-sink functions to high OC loads in adjacent surface waters (Webb et al., 2019). This effect may be further exacerbated in high-energy beach STEs with high advective water throughput, which prevent efficient accumulation of DOC.

We emphasize that on a qualitative level, the Spiekeroog beach STE is still a source of terrestrial, as well as recycled, chemically modified, marine DOM (**Supplementary Tables 1, 2** and **Figure 7**) to the nearshore water column. This modified DOM is enriched in humic-like FDOM and highly unsaturated compounds (**Supplementary Tables 1, 2**) and likely has contributed to the discharging inorganic nutrient pool, e.g., ammonium (Ahrens et al., 2020). In one of our runnel time series in March 2019, which took place shortly after the spring phytoplankton bloom, exfiltrating beach porewater appeared to be more labile (as indicated by Ideg) than the surrounding seawater, although it had less DOC (**Figure 8C**). This pattern was contradictory to our other results from the seasonal transects, as well as a runnel time series in September 2019 (**Figures 7**, **8**). It could imply that a lag in sedimentary microbial response during times of high coastal water column productivity causes inverse patterns of DOM degradation, i.e., a more labile DOM pool found in the porewaters compared to a less labile, more degraded DOM pool in the seawater. In addition, we cannot present any porewater exfiltration data from the low water line, because time-series sampling and seepage meter placement in a high-energy surf zone presents a formidable, yet-to-overcome challenge. However, future DOM characterization of SGD from the low water line will be necessary to fully elucidate the impact of Spiekeroog beach porewater onto the adjacent coastal North Sea.

CONCLUSION

Our study indicates that the Spiekeroog high-energy beach STE conveys chemically modified, terrestrial DOM from the inland freshwater lens to the coastal ocean. Terrestrial DOM seems to stem from the groundwater lens, partly being supplemented by vascular plant leachates from the dune belt. Overall, Spiekeroog beach appears to be a very active DOM turnover site, where dissolved, marine, and terrestrial OC can be remineralized with high efficiency, and where microbial degradation are imprinted onto the molecular composition of DOM of exfiltrating porewaters. Based on our data, we suggest that this high-energy beach STE is a net sink for OC from both the terrestrial as well as the marine realm. Furthermore, we propose the East Frisian barrier island beaches may act as efficient "digestors" of organic matter, perhaps respiring DOC also from many other coastal sources (i.e., rivers, tidal flats) found in their vicinity.

We emphasize that our study also revealed several research gaps, which contribute to uncertainties in data interpretation: (1) A characterization of deeper (>1 m) STE layers is needed to constrain endmember hydrochemistry. (2) A thorough investigation of particulate and sedimentary organic matter in the beach is necessary to complete the qualitative and quantitative OC budget. (3) An experimental setup is crucial to derive accurate microbial respiration rates, and to disentangle impacts of electron acceptors *vs.* electron donors on OC remineralization in this dynamic, high-energy environment. (4) An expansion of STE research from micro- and meso- to more macrotidal, exposed, high-energy coastlines is required to confirm the universality and thus global relevance of our findings.

DATA AVAILABILITY STATEMENT

Mass spectrometry and environmental data data are available on the open-access data repository PANGAEA (Waska 2021, Ahrens 2019).

AUTHOR CONTRIBUTIONS

HW designed the study, acquired the data, and wrote the manuscript. HS, SA, JG, JA, SS, and KS acquired the data and contributed to result interpretation and manuscript writing. OZ and TD contributed to study design and manuscript writing. All authors approved the submitted version.

FUNDING

This study was financed by the Niedersächsisches Ministerium für Wissenschaft und Kultur (MWK) in the scope of project "BIME" (ZN3184). SA acknowledges funding from the Max Planck Society.

ACKNOWLEDGMENTS

We would like to thank Swaantje Fock and Carsten Heithecker from Umweltzentrum Wittbülten, and Ulrike Seemann from Quellerdünenheim, for provision of onsite infrastructure. Joachim Ihnken from the Niedersächsische Landesbetrieb für Wasserwirtschaft, Küsten, und Naturschutz (NLWKN), Gregor Scheiffarth, Claus Schulz, and Lars Scheller from the Nationalpark Wattenmeer administration, and Helmo Nicolai from ICBM Terramare are thanked for their support with permits, onsite information, and onsite logistics. We are further grateful to the municipality of Spiekeroog, for accomodating and supporting basic research on the island. HW would like to thank Matthias Friebe, Ina Ulber, and Katrin Klaproth with assistance in field and lab work, and FT-ICR-MS analyses. The two reviewers are thanked for their detailed and constructive comments, which helped to improve this manuscript.

SUPPLEMENTARY MATERIAL

The Supplementary Material for this article can be found online at: https://www.frontiersin.org/articles/10.3389/fmars.2021.607083/full#supplementary-material

REFERENCES

Ahmerkamp, S., Winter, C., Krämer, K., Beer, D. D., Janssen, F., Friedrich, J., et al. (2017). Regulation of benthic oxygen fluxes in permeable sediments of the coastal ocean. *Limnol. Oceanogr.* 62, 1935–1954. doi: 10.1002/lno.10544

Ahrens, J. (2016). *Anorganisch-Geochemische Charakterisierung von Spiekerooger Strandsanden unter Anwendung der Sequentiellen Extraktion Von Eisen-Mineralphasen*. MSc thesis, University of Oldenburg, Oldenburg.

Ahrens, J., Beck, M., Marchant, H. K., Ahmerkamp, S., Schnetger, B., and Brumsack, H. J. (2020). Seasonality of organic matter degradation regulates nutrient and metal net fluxes in a high energy sandy beach. *J. Geophys. Res. Biogeosci.* 125:e2019JG005399.

Anderson, T. R., Rowe, E. C., Polimene, L., Tipping, E., Evans, C. D., Barry, C. D. G., et al. (2019). Unified concepts for understanding and modelling turnover of dissolved organic matter from freshwaters to the ocean: the UniDOM model. *Biogeochemistry* 146, 105–123. doi: 10.1007/s10533-019-00621-1

Anschutz, P., Charbonnier, C., Deborde, J., Deirmendjian, L., Poirier, D., Mouret, A., et al. (2016). Terrestrial groundwater and nutrient discharge along the 240-km-long Aquitanian coast. *Mar. Chem.* 185, 38–47. doi: 10.1016/j.marchem.2016.04.002

Anschutz, P., Smith, T., Mouret, A., Deborde, J., Bujan, S., Poirier, D., et al. (2009). Tidal sands as biogeochemical reactors. *Estuar. Coast. Shelf Sci.* 84, 84–90. doi: 10.1016/j.ecss.2009.06.015

Beck, M., Reckhardt, A., Amelsberg, J., Bartholomä, A., Brumsack, H. J., Cypionka, H., et al. (2017). The drivers of biogeochemistry in beach ecosystems: a cross-shore transect from the dunes to the low-water line. *Mar. Chem.* 190, 35–50. doi: 10.1016/j.marchem.2017.01.001

Benner, R., and Amon, R. M. (2015). The size-reactivity continuum of major bioelements in the ocean. *Ann. Rev. Mar. Sci.* 7, 185–205. doi: 10.1146/annurev-marine-010213-135126

Bianchi, T. S. (2011). The role of terrestrially derived organic carbon in the coastal ocean: a changing paradigm and the priming effect. *Proc. Natl. Acad. Sci. U.S.A.* 108, 19473–19481. doi: 10.1073/pnas.1017982108

Billerbeck, M., Werner, U., Polerecky, L., Walpersdorf, E., DeBeer, D., and Huettel, M. (2006). Surficial and deep pore water circulation governs spatial and temporal scales of nutrient recycling in intertidal sand flat sediment. *Mar. Ecol. Prog. Ser.* 326, 61–76. doi: 10.3354/meps326061

Charbonnier, C., Anschutz, P., Poirier, D., Bujan, S., and Lecroart, P. (2013). Aerobic respiration in a high-energy sandy beach. *Mar. Chem.* 155, 10–21. doi: 10.1016/j.marchem.2013.05.003

Charette, M. A., and Sholkovitz, E. R. (2006). Trace element cycling in a subterranean estuary: Part 2. geochemistry of the pore water. *Geochim. Cosmochim. Acta* 70, 811–826. doi: 10.1016/j.gca.2005.10.019

Couturier, M., Nozais, C., and Chaillou, G. (2016). Microtidal subterranean estuaries as a source of fresh terrestrial dissolved organic matter to the coastal ocean. *Mar. Chem.* 186, 46–57. doi: 10.1016/j.marchem.2016.08.001

D'Andrilli, J., Cooper, W. T., Foreman, C. M., and Marshall, A. G. (2015). An ultrahigh-resolution mass spectrometry index to estimate natural organic matter lability. *Rapid Commun. Mass. Spectrom.* 29, 2385–2401. doi: 10.1002/rcm.7400

Degenhardt, J., Dlugosch, L., Ahrens, J., Beck, M., Waska, H., and Engelen, B. (2020). Seasonal dynamics of microbial diversity at a sandy high energy beach reveal a resilient core community. *Front. Mar. Sci.* 7:869. doi: 10.3389/fmars.2020.573570

Dittmar, T., Koch, B., Hertkorn, N., and Kattner, G. (2008). A simple and efficient method for the solid-phase extraction of dissolved organic matter (SPE-DOM) from seawater. *Limnol. Oceanogr. Methods* 6, 230–235. doi: 10.4319/lom.2008.6.230

Ehlert, C., Reckhardt, A., Greskowiak, J., Liguori, B. T., Böning, P., Paffrath, R., et al. (2016). Transformation of silicon in a sandy beach ecosystem: Insights from stable silicon isotopes from fresh and saline groundwaters. *Chem. Geol.* 440, 207–218. doi: 10.1016/j.chemgeo.2016.07.015

Flerus, R., Lechtenfeld, O. J., Koch, B. P., McCallister, S. L., Schmitt-Kopplin, P., Benner, R., et al. (2012). A molecular perspective on the ageing of marine dissolved organic matter. *Biogeosciences* 9, 1935–1955. doi: 10.5194/bg-9-1935-2012

Froelich, P. N., Klinkhammer, G. P., Bender, M. L., Luedtke, N. A., Heath, G. R., Cullen, D., et al. (1979). Early oxidation of organic matter in pelagic sediments of the eastern equatorial Atlantic: suboxic diagenesis. *Geochim. Cosmochim. Acta* 43, 1075–1090. doi: 10.1016/0016-7037(79)90095-4

Goñi, M. A., and Gardner, I. R. (2003). Seasonal dynamics in dissolved organic carbon concentrations in a coastal water-table aquifer at the forest-marsh interface. *Aquat. Geochem.* 9, 209–232. doi: 10.1023/b:aqua.0000022955.82700.ed

Grasshoff, K., Kremling, K., and Erhardt, M. (1999). *Methods of Seawater Analysis*. Weinheim: Wiley-VCH.

Grünenbaum, N., Greskowiak, J., Sültenfuß, J., and Massmann, G. (2020). Groundwater flow and residence times below a meso-tidal high-energy beach: a model-based analyses of salinity patterns and 3H-3He groundwater ages. *J. Hydrol.* 2020:124948. doi: 10.1016/j.jhydrol.2020.124948

Ibánhez, J. S. P., and Rocha, C. (2016). oxygen transport and reactivity within a sandy seepage face in a mesotidal lagoon (Ria Formosa, Southwestern Iberia). *Limnol. Oceanogr.* 61, 61–77. doi: 10.1002/lno.10199

Itaya, K., and Ui, M. (1966). A new micromethod for the colorimetric determination of inorganic phosphate. *Clin. Chim. Acta* 14, 361–366. doi: 10.1016/0009-8981(66)90114-8

Jiang, S., Zhang, Y., Jin, J., Wu, Y., Wei, Y., Wang, X., et al. (2020). Organic carbon in a seepage face of a subterranean estuary: Turnover and microbial interrelations. *Sci. Total Environ.* 725:138220. doi: 10.1016/j.scitotenv.2020.138220

Kaiser, K., and Guggenberger, G. (2000). The role of DOM sorption to mineral surfaces in the preservation of organic matter in soils. *Organ. Geochem.* 31, 711–725. doi: 10.1016/s0146-6380(00)00046-2

Kim, J., and Kim, G. (2017). Inputs of humic fluorescent dissolved organic matter via submarine groundwater discharge to coastal waters off a volcanic island (Jeju, Korea). *Sci. Rep.* 7, 1–9.

Kim, K. H., Michael, H. A., Field, E. K., and Ullman, W. J. (2019). Hydrologic shifts create complex transient distributions of particulate organic carbon and biogeochemical responses in beach aquifers. *J. Geophys. Res. Biogeosci.* 124, 3024–3038. doi: 10.1029/2019jg005114

Kim, T. H., Waska, H., Kwon, E., Suryaputra, I. G. N., and Kim, G. (2012). Production, degradation, and flux of dissolved organic matter in the subterranean estuary of a large tidal flat. *Mar. Chem.* 142, 1–10. doi: 10.1016/j.marchem.2012.08.002

Koch, B. P., and Dittmar, T. (2006). From mass to structure: An aromaticity index for high-resolution mass data of natural organic matter. *Rapid Commun. Mass Spectrom.* 20, 926–932. doi: 10.1002/rcm.2386

Kwon, E. Y., Kim, G., Primeau, F., Moore, W. S., Cho, H. M., DeVries, T., et al. (2014). Global estimate of submarine groundwater discharge based on an observationally constrained radium isotope model. *Geophys. Res. Lett.* 41, 8438–8444. doi: 10.1002/2014gl061574

Lalonde, K., Mucci, A., Ouellet, A., and Gélinas, Y. (2012). Preservation of organic matter in sediments promoted by iron. *Nature* 483, 198–200. doi: 10.1038/nature10855

Laskov, C., Herzog, C., Lewandowski, J., and Hupfer, M. (2007). Miniaturized photometrical methods for the rapid analysis of phosphate, ammonium, ferrous iron, and sulfate in pore water of freshwater sediments. *Limnol. Oceanog. Methods* 5, 63–71. doi: 10.4319/lom.2007.5.63

Lechtenfeld, O. J., Kattner, G., Flerus, R., McCallister, S. L., Schmitt-Kopplin, P., and Koch, B. P. (2014). Molecular transformation and degradation of refractory dissolved organic matter in the Atlantic and Southern Ocean. *Geochim. Cosmochim. Acta* 126, 321–337. doi: 10.1016/j.gca.2013.11.009

Linkhorst, A., Dittmar, T., and Waska, H. (2017). Molecular fractionation of dissolved organic matter in a shallow subterranean estuary: the role of the iron curtain. *Environm. Sci. Technol.* 51, 1312–1320. doi: 10.1021/acs.est.6b03608

Luijendijk, E., Gleeson, T., and Moosdorf, N. (2020). Fresh groundwater discharge insignificant for the world's oceans but important for coastal ecosystems. *Nat. Commun.* 11, 1–12. doi: 10.1007/1-4020-4738-x_1

Ma, Q., and Zhang, Y. (2020). Global research trends and hotspots on submarine groundwater discharge (SGD): a bibliometric analysis. *Intern. J. Environ. Res. Public Health* 17:830. doi: 10.3390/ijerph17030830

McAllister, S. M., Barnett, J. M., Heiss, J. W., Findlay, A. J., MacDonald, D. J., Dow, C. L., et al. (2015). Dynamic hydrologic and biogeochemical processes drive microbially enhanced iron and sulfur cycling within the intertidal mixing zone of a beach aquifer. *Limnol. Oceanogr.* 60, 329–345. doi: 10.1002/lno.10029

McDonough, L. K., O'Carroll, D. M., Meredith, K., Andersen, M. S., Brugger, C., Huang, H., et al. (2020a). Rainfall recharge drives groundwater dissolved organic matter composition in acoastal sand aquifer. *Water Res.* 169:115201. doi: 10.1016/j.watres.2019.115201

McDonough, L. K., Rutlidge, H., O'Carroll, D. M., Andersen, M. S., Meredith, K., Behnke, M., et al. (2020b). Characterisation of shallow groundwater dissolved organic matter in aeolian, alluvial and fractured rock aquifers. *Geochim. Cosmochim. Acta* 273, 163–176. doi: 10.1016/j.gca.2020.01.022

McDonough, L. K., Santos, I. R., Andersen, M. S., O'Carroll, D. M., Rutlidge, H., Meredith, K., et al. (2020c). Changes in global groundwater organic carbon driven by climate change and urbanization. *Nat. Commun.* 11:1279.

McLachlan, A. (1982). A model for the estimation of water filtration and nutrient regeneration by exposed sandy beaches. *Mar. Environ. Res.* 6, 37–47. doi: 10.1016/0141-1136(82)90006-x

Medeiros, P. M., Seidel, M., Niggemann, J., Spencer, R. G., Hernes, P. J., Yager, P. L., et al. (2016). A novel molecular approach for tracing terrigenous dissolved organic matter into the deep ocean. *Glob. Biogeochem. Cycles* 30, 689–699. doi: 10.1002/2015gb005320

Merder, J., Freund, J. A., Feudel, U., Hansen, C. T., Hawkes, J. A., Jacob, B., et al. (2020). ICBM-OCEAN: processing ultrahigh-resolution mass spectrometry data of complex molecular mixtures. *Analyt. Chem.* 92, 6832–6838. doi: 10.1021/acs.analchem.9b05659

Meredith, K. T., Baker, A., Andersen, M. S., O'Carroll, D., Rutlidge, H., McDonough, L. K., et al. (2020). Isotopic and chromatographic fingerprinting of the sources of dissolved organic carbon in a shallow coastal aquifer. *Hydrol. Earth Syst. Sci.* 24, 2167–2178. doi: 10.5194/hess-24-2167-2020

Moore, W. S. (1999). The subterranean estuary: a reaction zone of ground water and sea water. *Mar. Chem.* 65, 111–125. doi: 10.1016/s0304-4203(99)00014-6

Mostovaya, A., Hawkes, J. A., Dittmar, T., and Tranvik, L. J. (2017). Molecular determinants of dissolved organic matter reactivity in lake water. *Front. Earth Sci.* 5:106. doi: 10.3389/feart.2017.00106

Nelson, C. E., Donahue, M. J., Dulaiova, H., Goldberg, S. J., La Valle, F. F., Lubarsky, K., et al. (2015). Fluorescent dissolved organic matter as a multivariate biogeochemical tracer of submarine groundwater discharge in coral reef ecosystems. *Mar. Chem.* 177, 232–243. doi: 10.1016/j.marchem.2015.06.026

Novitsky, J. A., and MacSween, M. C. (1989). Microbiology of a high energy beach sediment: evidence for an active and growing community. *Mar. Ecol. Prog. Ser.* 52, 71–75. doi: 10.3354/meps052071

Oehler, T., Tamborski, J., Rahman, S., Moosdorf, N., Ahrens, J., Mori, C., et al. (2019). DSi as a tracer for submarine groundwater discharge. *Front. Mar. Sci.* 6:563. doi: 10.3389/fmars.2019.00563

Oksanen, J., Blanchet, F. G., Kindt, R., Legendre, P., McGlinn, D., Minchin, P. R., et al. (2013). Package 'vegan'. *Commun. Ecol. Pack. Vers.* 2, 1–295.

Osterholz, H., Niggemann, J., Giebel, H. A., Simon, M., and Dittmar, T. (2015). Inefficient microbial production of refractory dissolved organic matter in the ocean. *Nat. Commun.* 6, 1–8.

Paffrath, R., Pahnke, K., Behrens, M. K., Reckhardt, A., Ehlert, C., Schnetger, B., et al. (2020). Rare earth element behavior in a sandy subterranean estuary of the southern North Sea. *Front. Mar. Sci.* 7:424. doi: 10.3389/fmars.2020.00424

Reckhardt, A., Beck, M., Greskowiak, J., Schnetger, B., Boettcher, M. E., Gehre, M., et al. (2017). Cycling of redox-sensitive elements in a sandy subterranean estuary of the southern North Sea. *Mar. Chem.* 188, 6–17. doi: 10.1016/j.marchem.2016.11.003

Reckhardt, A., Beck, M., Seidel, M., Riedel, T., Wehrmann, A., Bartholomä, A., et al. (2015). Carbon, nutrient, and trace metal cycling in sandy sediments: a comparison of high-energy beaches and backbarrier tidal flats. *Estuar. Coast. Shelf Sci.* 159, 1–14. doi: 10.1016/j.ecss.2015.03.025

Riedel, T., Biester, H., and Dittmar, T. (2012). Molecular fractionation of dissolved organic matter with metal salts. *Environ. Sci. Technol.* 46, 4419–4426. doi: 10.1021/es203901u

Robinson, C., Gibbes, B., and Li, L. (2006). Driving mechanisms for groundwater flow and salt transport in a subterranean estuary. *Geophys. Res. Lett.* 33:L03402. doi: 10.1029/2005GL025247

Rocha, C. (2008). Sandy sediments as active biogeochemical reactors: compound cycling in the fast lane. *Aquat. Microb. Ecol.* 53, 119–127. doi: 10.3354/ame01221

Röper, T., Kröger, K. F., Meyer, H., Sültenfuss, J., Greskowiak, J., and Massmann, G. (2012). Groundwater ages, recharge conditions and hydrochemical evolution of a barrier island freshwater lens (Spiekeroog, Northern Germany). *J. Hydrol.* 454, 173–186. doi: 10.1016/j.jhydrol.2012.06.011

Roy, M., Martin, J. B., Cherrier, J., Cable, J. E., and Smith, C. G. (2010). Influence of sea level rise on iron diagenesis in an east Florida subterranean estuary. *Geochim. Cosmochim. Acta* 74, 5560–5573. doi: 10.1016/j.gca.2010.07.007

Roy, M., Martin, J. B., Smith, C. G., and Cable, J. E. (2011). Reactive-transport modeling of iron diagenesis and associated organic carbon remineralization in a Florida (USA) subterranean estuary. *Earth Planet. Sci. Lett.* 304, 191–201. doi: 10.1016/j.epsl.2011.02.002

Santos, I. R., Burnett, W. C., Dittmar, T., Suryaputra, I. G. N. A., and Chanton, J. (2009). Tidal pumping drives nutrient and dissolved organic matter dynamics in a Gulf of Mexico subterranean estuary. *Geochim. Cosmochim. Acta* 73, 1325–1339. doi: 10.1016/j.gca.2008.11.029

Santos, I. R., Eyre, B. D., and Huettel, M. (2012). The driving forces of porewater and groundwater flow in permeable coastal sediments: a review. *Estuar. Coast. Shelf Sci.* 98, 1–15. doi: 10.1016/j.ecss.2011.10.024

Sarazin, G., Michard, G., and Prevot, F. (1999). A rapid and accurate spectroscopic method for alkalinity measurements in sea water samples. *Water Res.* 33, 290–294. doi: 10.1016/s0043-1354(98)00168-7

Seibert, S. L., Böttcher, M. E., Schubert, F., Pollmann, T., Giani, L., Tsukamoto, S., et al. (2019a). Iron sulfide formation in young and rapidly-deposited permeable sands at the land-sea transition zone. *Sci. Total Environ.* 649, 264–283. doi: 10.1016/j.scitotenv.2018.08.278

Seibert, S. L., Greskowiak, J., Prommer, H., Böttcher, M. E., and Massmann, G. (2019b). Modeling of biogeochemical processes in a barrier island freshwater lens (Spiekeroog, Germany). *J. Hydrol.* 575, 1133–1144. doi: 10.1016/j.jhydrol.2019.05.094

Seibert, S. L., Holt, T., Reckhardt, A., Ahrens, J., Beck, M., Pollmann, T., et al. (2018). Hydrochemical evolution of a freshwater lens below a barrier island (Spiekeroog, Germany): the role of carbonate mineral reactions, cation exchange and redox processes. *Appl. Geochem.* 92, 196–208. doi: 10.1016/j.apgeochem.2018.03.001

Seibt, M. (2017). *The Molecular Geography of Dissolved Organic Matter in the Atlantic and Southern Ocean*. Ph.D. thesis, University of Oldenburg, Oldenburg.

Seidel, M., Beck, M., Greskowiak, J., Riedel, T., Waska, H., Suryaputra, I. G. N. A., et al. (2015). Benthic-pelagic coupling of nutrients and dissolved organic matter composition in an intertidal sandy beach. *Mar. Chem.* 176, 150–163. doi: 10.1016/j.marchem.2015.08.011

Seidel, M., Beck, M., Riedel, T., Waska, H., Suryaputra, I. G., Schnetger, B., et al. (2014). Biogeochemistry of dissolved organic matter in an anoxic intertidal creek bank. *Geochimi. Cosmochim. Acta* 140, 418–434. doi: 10.1016/j.gca.2014.05.038

Shen, Y., Chapelle, F. H., Strom, E. W., and Benner, R. (2015). Origins and bioavailability of dissolved organic matter in groundwater. *Biogeochemistry* 122, 61–78. doi: 10.1007/s10533-014-0029-4

Sirois, M., Couturier, M., Barber, A., Gélinas, Y., and Chaillou, G. (2018). Interactions between iron and organic carbon in a sandy beach subterranean estuary. *Mar. Chem.* 202:86. doi: 10.1016/j.marchem.2018.02.004

Spiteri, C., Slomp, C. P., Charette, M. A., Tuncay, K., and Meile, C. (2008). Flow and nutrient dynamics in a subterranean estuary (Waquoit Bay, MA, USA): field data and reactive transport modeling. *Geochim. Cosmochim. Acta* 72, 3398–3412. doi: 10.1016/j.gca.2008.04.027

Streif, H. (2002). "The Pleistocene and Holocene development of the southeastern North Sea basin and adjacent coastal areas," in *Climate Development and History of the North Atlantic Realm*, eds G. Wefer, W. Berger, K.-E. Behre, and E. Jansen (Berlin: Springer), 387–397. doi: 10.1007/978-3-662-04965-5_25

Suryaputra, I. G. N. A., Santos, I. R., Huettel, M., Burnett, W. C., and Dittmar, T. (2015). Non-conservative behavior of fluorescent dissolved organic matter (FDOM) within a subterranean estuary. *Continent. Shelf Res.* 110, 183–190. doi: 10.1016/j.csr.2015.10.011

Van Cappellen, P., and Wang, Y. (1996). Cycling of iron and manganese in surface sediments; a general theory for the coupled transport and reaction of carbon, oxygen, nitrogen, sulfur, iron, and manganese. *Ame. J. Sci.* 296, 197–243. doi: 10.2475/ajs.296.3.197

Waska, H., Brumsack, H. J., Massmann, G., Koschinsky, A., Schnetger, B., Simon, H., et al. (2019a). Inorganic and organic iron and copper species of the subterranean estuary: Origins and fate. *Geochim. Cosmochim. Acta* 259, 211–232. doi: 10.1016/j.gca.2019.06.004

Waska, H., Greskowiak, J., Ahrens, J., Beck, M., Ahmerkamp, S., Böning, P., et al. (2019b). Spatial and temporal patterns of pore water chemistry in the inter-tidal zone of a high energy beach. *Front. Mar. Sci.* 6:154. doi: 10.3389/fmars.2019.00154

Webb, J. R., Santos, I. R., Maher, D. T., Tait, D. R., Cyronak, T., Sadat-Noori, M., et al. (2019). Groundwater as a source of dissolved organic matter to coastal waters: insights from radon and CDOM observations in 12 shallow coastal systems. *Limnol. Oceanogr.* 64, 182–196. doi: 10.1002/lno.11028

Yang, L., Chen, C. T. A., Hong, H., Chang, Y. C., and Lui, H. K. (2015). Mixing behavior and bioavailability of dissolved organic matter in two contrasting subterranean estuaries as revealed by fluorescence spectroscopy and parallel factor analysis. *Estuar. Coas. Shelf Sci.* 166, 161–169. doi: 10.1016/j.ecss.2014.10.018

Conflict of Interest: The authors declare that the research was conducted in the absence of any commercial or financial relationships that could be construed as a potential conflict of interest.

The handling editor is currently organizing a Research Topic with one of the authors HW.